

High Energy Spectral Components in Gamma-Ray Burst Afterglows

Bing Zhang & Peter Mészáros

Astronomy & Astrophysics Dept., Pennsylvania State University, University Park, PA 16803

ABSTRACT

We investigate two high energy radiation mechanisms, the proton synchrotron and the electron inverse Compton emission, and explore their possible signatures in the broad-band spectra and in the keV to GeV light curves of gamma-ray burst afterglows. We develop a simple analytical approach, allowing also for the effects of photon-photon pair production, and explore the conditions under which one or the other of these components dominates. We find that the parameter space region where the proton synchrotron and other hadron-related emission components dominate is small, while the parameter space region where the electron inverse Compton component dominates is quite substantial, as is also a third region where the electron synchrotron dominates. We discuss the prospects and astrophysical implications of directly detecting the inverse Compton and the proton high energy components in various bands, in particular in the GeV band with future missions such as *GLAST*, and in the X-ray band with *Chandra*.

Subject headings: gamma rays: bursts - radiation mechanisms: non-thermal

1. Introduction

Gamma-ray Burst (GRB) afterglows have been detected mainly at longer wavebands, from X-rays to radio, extending up to months after the burst triggers (e.g. van Paradijs, Kouveliotou & Wijers 2000). These long-lived afterglow emissions are generally interpreted within the fireball shock model by the synchrotron emission of external shock-accelerated relativistic electrons. The broadband electron synchrotron spectrum (Sari, Piran & Narayan 1998) has proven to be a useful paradigm to study afterglow lightcurves in the X-ray, optical, and radio band, and to constrain various unknown parameters. On the other hand, there are other high energy emission components, whose role in determining the long wavelength afterglows may be secondary or of limited duration, but which may for some time dominate the high energy, X-ray to GeV spectrum of the afterglows. These include the synchrotron self-inverse Compton emission (IC) of the electrons (Mészáros, Rees & Papathanassiou 1994; Waxman 1997; Panaitescu & Mészáros 1998; Wei & Lu 1998, 2000; Dermer, Böttcher & Chiang 2000a; Dermer, Chiang & Mitman 2000b; Panaitescu & Kumar 2000; Sari & Esin 2001), the proton synchrotron emission (Vietri 1997; Böttcher & Dermer 1998; Totani 1998) as well as some other hadron-related emission components (Böttcher & Dermer 1998). The emission from such high energy mechanisms in the GeV band

may have been detected by *EGRET* in GRB 940217 (Hurley et al. 1994) and probably also in some other GRBs, and will be detectable by next generation GeV γ -ray missions such as *GLAST*. In the X-ray band, the electron IC component has been pointed out as potentially detectable at a later time (Sari & Esin 2001).

Previous afterglow snapshot spectral fits to multi-wavelength data up to X-rays (e.g. Wijers & Galama, 1999; Panaiteescu & Kumar 2000; van Paradijs, Kouveliotou & Wijers, 2000; Freedman & Waxman 2001) have constrained some of the fireball shock parameters (e.g. the electron and magnetic field energy equipartition parameters ϵ_e , ϵ_B), which are found to vary over a wide range. Because of the relative looseness of these fits, there is a need to tighten the model constraints. A promising way to do this is by extending upward the frequency range over which the snapshot spectra are fitted, and to investigate the relative importance and additional constraints imposed by these high energy radiation components, over a wider region of parameter phase space, which is the subject of this paper. For this purpose, we use a simple analytic approach to describe the various spectral components. Following a brief general treatment of the particle distribution and the synchrotron spectrum of the electrons (§2), we discuss the proton synchrotron spectral component (§3) and the electron inverse Compton component (§4), and compare their importance relative to the electron synchrotron emission in the frequency regime below the electron synchrotron cut-off. Above this cut-off, the relative importance between the electron’s IC and the hadron-related components is also discussed. In §5 we incorporate the high energy absorption due to $\gamma - \gamma$ pair production in an analytic manner. We then present several examples of the broad band spectra of GRB afterglows within different parameter regimes in §6, and discuss the detectability of these high energy spectral components within various bands, especially in the X-ray band and the GeV band. Finally we summarize our findings in §7.

2. Proton and electron distributions and cooling

We assume that for negligible radiative losses both electrons and protons are shock accelerated to a single relativistic power law distribution of index p . Denoting the particle species by the subindex “x” (which indicates “e” for electrons and “p” for protons), after a certain time the particle distribution becomes a broken power law depending on the relative ordering between the injection minimum energy, $\gamma_{m,x}$, and the energy at which the particles cool radiatively in an expansion timescale, $\gamma_{c,x}$. Given a maximum particle energy $\gamma_{u,x}$ at which the acceleration time equals the energy loss time, the particle distribution is $N(\gamma_x) \propto \gamma_x^{-p}$ for $\gamma_{m,x} < \gamma_x < \gamma_{c,x}$, and $N(\gamma_x) \propto \gamma_x^{-p-1}$ for $\gamma_{c,x} < \gamma_x < \gamma_{u,x}$, if $\gamma_{m,x} < \gamma_{c,x}$ (slow cooling regime); and is $N(\gamma_x) \propto \gamma_x^{-2}$ for $\gamma_{c,x} < \gamma_x < \gamma_{m,x}$, and $N(\gamma_x) \propto \gamma_x^{-p-1}$ for $\gamma_{m,x} < \gamma_x < \gamma_{u,x}$, if $\gamma_{m,x} > \gamma_{c,x}$ (fast cooling regime). For $p > 2$, the mean particle energy is $\bar{\gamma}_x = [(p-1)/(p-2)]\gamma_{m,x}$. Hereafter we assume for simplicity the same power law index p for both electrons and protons. Assuming that $\zeta_p n$ and $\zeta_e n$ are the number densities of the shock-accelerated power-law protons and electrons, respectively, where ζ_p and ζ_e are the injection fractions and n is the number density of the pre-shock thermal medium,

one can define the energy portion contained in the power-law distributed electrons and protons with respect to the total energy behind the shock to be $\epsilon_e = \zeta_e(m_e/m_p)(\bar{\gamma}_e/\Gamma)$, and $\epsilon_p = \zeta_p(\bar{\gamma}_p/\Gamma)$, respectively, where Γ is the bulk Lorentz factor of the blast wave. Consequently, the minimum energy for the power-law distributed electrons and the protons are¹

$$\gamma_{m,e} = \left(\frac{\epsilon_e}{\zeta_e}\right) \left(\frac{m_p}{m_e}\right) \left(\frac{p-2}{p-1}\right) \Gamma, \quad \gamma_{m,p} = \left(\frac{\epsilon_p}{\zeta_p}\right) \left(\frac{p-2}{p-1}\right) \Gamma. \quad (1)$$

The above equations are for $p > 2$, which for simplicity will be assumed to be valid. For p getting closer to 2, the $(p-2)/(p-1)$ factor is no longer precise, and when $p = 2$, it is replaced by $\ln^{-1}(\gamma_{u,x}/\gamma_{m,x})$. However, the imprecise of eq.(1) at $p = 2$ does not influence the precise of the discussions in §3 (e.g. eq.[2]) since both correction factors for the proton and the electron components are cancelled out. The cooling energy $\gamma_{c,x}$ is defined by equating the comoving adiabatic expansion time $t'_{ad} \sim r/(\Gamma c) \sim \Gamma t$ (where Γ is the bulk Lorentz factor of the blastwave at the radius r , $t \sim \Gamma^{-2}(r/c)$ is the expansion time in the observer frame) to the comoving radiation cooling time $t'_c = [(t'_{sy})^{-1} + (t'_{IC})^{-1}]^{-1} = t'_{sy}/(1+Y)$, where t'_{sy} and t'_{IC} are the synchrotron and the IC cooling time, and $Y = t'_{sy}/t'_{IC} = (-1 + \sqrt{1 + 4\eta\epsilon_x/\epsilon_B})/2$ is the Compton factor (e.g. Panaiteescu & Kumar 2000; Sari & Esin 2001). Here redshift corrections have been ignored for simplicity, $\eta = \text{Min}[1, (\gamma_{m,x}/\gamma_{c,x})^{p-2}]$ is the fraction of the particle energy that is radiated away via both synchrotron and inverse Compton (Sari & Esin 2001), and ϵ_B is the fraction of the magnetic energy density with respect to the total energy density behind the shock, so that the comoving magnetic field $B' = \Gamma c(32\pi n m_p \epsilon_B)^{1/2}$. For $\eta\epsilon_x/\epsilon_B \ll 1$, one has $Y \sim \eta\epsilon_x/\epsilon_B \ll 1$ and $t'_c \sim t'_{sy}$, and the IC cooling is not important. Alternatively, when $\eta\epsilon_x/\epsilon_B \gg 1$, IC cooling is important, and $t'_c \sim (\eta\epsilon_e/\epsilon_B)^{-1/2} t'_{sy}$ (Sari & Esin 2001). The critical energy above which the particle species x cool in an expansion time is $\gamma_{c,x} = (1+Y_x)^{-1}(6\pi m_x c/\Gamma \sigma_{T,x} B'^2 t)$, where $t'_{sy} = (\gamma_x m_x c^2)/[(4/3)\sigma_{T,x} c \gamma_x^2 (B'^2/8\pi)]$ is used, $\sigma_{T,x} = (8\pi/3)(e^2/m_x c^2)^2$ is the Thomson cross section for particles of mass m_x , and $\sigma_{T,p}/\sigma_{T,e} = (m_e/m_p)^2$.

The maximum energy $\gamma_{u,x}$ is defined by equating the comoving acceleration time $t'_{acc} \equiv 2\pi\alpha r_L/c = 2\pi\alpha\gamma_{u,x} m_x c/eB'$ (where r_L is the Larmor radius, and α is a factor of the order of unity for relativistic shocks) to the minimum of the comoving adiabatic cooling time t'_{ad} and the comoving radiation cooling time t'_c . This gives $\gamma_{u,x} = \text{Min}\{(2\pi\alpha)^{-1}(eB'/m_x c)(\Gamma t), [3e/\alpha B' \sigma_{T,x} (1+Y_x)]^{1/2}\}$, where for protons the first part of the equation applies, while for the electrons it is the latter.

The electron synchrotron emission spectrum is a broken power law separated by three characteristic frequencies: the self-absorption frequency $\nu_{a,e}$, the characteristic frequency for the minimum energy particles, $\nu_{m,e} \simeq (\frac{4}{3}\Gamma) \frac{3}{4\pi} \frac{eB'}{m_e c} \gamma_{m,e}^2$, and the cooling frequency, $\nu_{c,e} \simeq (\frac{4}{3}\Gamma) \frac{3}{4\pi} \frac{eB'}{m_e c} \gamma_{c,e}^2$. Similar expressions apply for protons, except that synchrotron absorption and cooling are less

¹We note that the larger minimum proton energy estimates $\gamma_{m,p} = \Gamma$ adopted, e.g., by Vietri 1997; Böttcher & Dermer 1998 and Totani 1998, when p is close to 2 as assumed in those references, lead to larger proton synchrotron flux levels than those obtained using equation (1), because of the higher $\bar{\gamma}_p$ involved.

important than in electrons. For both p and e the maximum particle energy $\gamma_{u,x}$ defines a synchrotron cut-off frequency $\nu_{u,x} \simeq (\frac{4}{3}\Gamma)\frac{3}{4\pi}\frac{eB'}{m_x c}\gamma_{u,x}^2$. In the above expressions, the factor (4/3) gives a more precise conversion from the comoving frame to the observer frame (Wijers & Galama 1999). The spectral indices of the four segments ordering from low to high in frequency are [2, 1/3, -1/2, -p/2] for the fast-cooling ($\nu_{c,e} < \nu_{m,e}$) regime, or [2, 1/3, -(p-1)/2, -p/2] for the slow-cooling ($\nu_{c,e} > \nu_{m,e}$) regime, respectively (Sari et al. 1998).

3. Synchrotron components

A potentially interesting high energy emission component of GRB afterglows is the synchrotron emission from the shock-accelerated relativistic protons (Vietri 1997; Böttcher & Dermer 1998; Totani 1998, 2000). Compared to electrons, the protons are inefficient emitters due to their much larger mass. The ratio of the characteristic synchrotron frequencies of protons and electrons is

$$\frac{\nu_{m,p}}{\nu_{m,e}} = \left(\frac{\gamma_{m,p}}{\gamma_{m,e}}\right)^2 \left(\frac{m_e}{m_p}\right) = \left(\frac{\epsilon_p/\zeta_p}{\epsilon_e/\zeta_e}\right)^2 \left(\frac{m_e}{m_p}\right)^3, \quad (2)$$

where eq.(1) is used. The peak synchrotron flux for the emission of particle x is $F_{\nu,max,x} \propto n_x P'_{\nu'_{m,x}} \propto n_x/m_x$, where $P'_{\nu'_{m,x}} = \phi_o(\sqrt{3}e^3 B'/m_x c^2)$, and $\phi_o \sim 0.6$ (Wijers & Galama, 1999). This is independent of whether the peak is at $\nu_{m,x}$ or at $\nu_{c,x}$. Thus the ratio of the peak flux of the two particle species is

$$\frac{F_{\nu,max,p}}{F_{\nu,max,e}} = \left(\frac{\zeta_p}{\zeta_e}\right) \left(\frac{m_e}{m_p}\right). \quad (3)$$

We see that both $\nu_{m,p}$ and $F_{\nu,max,p}$ are much smaller than $\nu_{m,e}$ and $F_{\nu,max,e}$, respectively, indicating that the proton emission component is usually buried under the electron emission component. However, the ratio of the cooling frequencies is

$$\frac{\nu_{c,p}}{\nu_{c,e}} = \left(\frac{1+Y_e}{1+Y_p}\right)^2 \left(\frac{m_p}{m_e}\right)^6 \quad (4)$$

(see §2), which means that protons barely cool while electrons cool rapidly. This allows, in some cases, the proton component to dominate over the electron component at high frequencies.

We consider now a certain observation band $\Delta\nu$ around ν which is above both the cooling frequency and the characteristic synchrotron frequency of the electrons, but is below the electrons' synchrotron cut-off frequency, i.e. $\nu_{c,e}$ (and $\nu_{m,e}$) $< \nu < \nu_{u,e}$. Regardless of the relative ordering of $\nu_{m,e}$ and $\nu_{c,e}$ (slow-cooling or fast cooling), the electron synchrotron flux at this frequency is $F_{\nu,e}(\nu) = (\nu/\nu_{m,e})^{-(p-1)/2} F_{\nu,max,e} \cdot (\nu_{c,e}/\nu)^{1/2}$. If $\nu < \nu_{u,p}$ is also satisfied, the flux of the proton synchrotron component at the same frequency is $F_{\nu,p}(\nu) = (\nu/\nu_{m,p})^{-(p-1)/2} F_{\nu,max,p}$, since

$\nu_{m,p} < \nu_{m,e}$ and usually $\nu_{c,p} \gtrsim \nu_{u,p}$. Thus

$$\frac{F_{\nu,p}(\nu)}{F_{\nu,e}(\nu)} = \left(\frac{F_{\nu,max,p}}{F_{\nu,max,e}} \right) \left(\frac{\nu_{m,p}}{\nu_{m,e}} \right)^{(p-1)/2} \left(\frac{\nu}{\nu_{c,e}} \right)^{1/2} = \left(\frac{\epsilon_p}{\epsilon_e} \right)^{(p-1)} \left(\frac{\zeta_e}{\zeta_p} \right)^{(p-2)} \left(\frac{m_e}{m_p} \right)^{(3p-1)/2} \left(\frac{\nu}{\nu_{c,e}} \right)^{1/2}. \quad (5)$$

We see that ν must be $\gg \nu_{c,e}$ to make the proton component show up in the spectrum, and that a large ϵ_p and a small ϵ_e favor the proton component. The dependence on the injection parameters ζ_e and ζ_p is weak for p close to 2.

For the purposes of numerical examples we use below a standard scenario (e.g. Mészáros & Rees 1997) in which a blast wave with total energy per solid angle $\mathcal{E} = E/\Omega = 10^{52}$ ergs/Sr \mathcal{E}_{52} expands into a uniform interstellar medium of particle number density $n \text{ cm}^{-3}$, and Ω is a putative jet opening solid angle. (In follows we will not discuss the jet dynamics. This does not influence our discussions on the early GeV afterglows, but may quantitatively, although not qualitatively, change the discussions of the late X-ray afterglows, if the transitions occur after the jet breaks. A wind-like external medium with $n \propto r^{-2}$ may be also incorporated in a similar way but we do not discuss this here). For the uniform external medium case, the blast wave starts to decelerate at a radius $r_{dec} \sim (3\mathcal{E}/4\pi n m_p c^2 \Gamma_0^2)^{1/3} \sim 2.6 \times 10^{16} \text{ cm } \mathcal{E}_{52}^{1/3} n^{-1/3} \Gamma_{0,300}^{-2/3}$, at an observer time $t_{dec} \sim (r_{dec}/4\Gamma_0^2 c) \cdot (1+z) \sim 2.4 \text{ s } \mathcal{E}_{52}^{1/3} n^{-1/3} \Gamma_{0,300}^{-8/3} (1+z) \text{ s}$. Here $\Gamma_0 = 300\Gamma_{0,300} = E/M_0 c^2$ is the initial bulk Lorentz factor of the shocked materials at $t = t_{dec}$ and the factor $(1+z)$ reflects the cosmological time dilation effect. After the external shocks has formed, the blast wave will be decelerated self-similarly and its advance is measured by $r(t) \sim [12\mathcal{E}ct/(1+z)/4\pi n m_p c^2]^{1/4} = 1.6 \times 10^{17} \text{ cm } (\mathcal{E}_{52}/n)^{1/4} [t_h/(1+z)]^{1/4}$, while the bulk Lorentz factor decays as $\Gamma(t) \sim [3\mathcal{E}(1+z)^3/4^3 \cdot 4\pi n m_p c^5 t^3]^{1/8} = 19.4(\mathcal{E}_{52}/n)^{1/8} [t_h/(1+z)]^{-3/8}$. Here $r = 4\Gamma^2 ct(1+z)$ has been adopted, and t_h is the earth observer time in unit of hours. The comoving magnetic field is $B' = 7.5 \text{ G } \epsilon_B^{1/2} \mathcal{E}_{52}^{1/8} n^{3/8} [t_h/(1+z)]^{-3/8} \text{ G}$. The breaks in the electron energy distribution are then given by

$$\gamma_{m,e} = 5.9 \times 10^3 (\epsilon_e/\zeta_e) (\mathcal{E}_{52}/n)^{1/8} [t_h/(1+z)]^{-3/8}, \quad (6)$$

$$\gamma_{c,e} = 1.96 \times 10^2 (1+Y_e)^{-1} \epsilon_B^{-1} \mathcal{E}_{52}^{-3/8} n^{-5/8} [t_h/(1+z)]^{1/8}. \quad (7)$$

In eq.(6) and hereafter $p = 2.2$ for both electrons and protons has been adopted to calculate numerically the coefficients. The p -dependences in the power indices, if necessary, will be still retained. The observed characteristic electron synchrotron frequency is then $\nu_{m,e} = 2.9 \times 10^{16} \text{ Hz } (\epsilon_e/\zeta_e)^2 \epsilon_B^{1/2} \mathcal{E}_{52}^{1/2} t_h^{-3/2} (1+z)^{1/2}$, while that for the protons is $\nu_{m,p} = 4.6 \times 10^6 \text{ Hz } (\epsilon_p/\zeta_p)^2 \epsilon_B^{1/2} \mathcal{E}_{52}^{1/2} t_h^{-3/2} (1+z)^{1/2}$. The electron cooling frequency is

$$\nu_{c,e} = 3.1 \times 10^{13} \text{ Hz } (1+Y_e)^{-2} \epsilon_B^{-3/2} \mathcal{E}_{52}^{-1/2} n^{-1} t_h^{-1/2} (1+z)^{-1/2}, \quad (8)$$

and the cut-off maximum frequencies for the electrons and the protons are

$$\nu_{u,e} = 2.3 \times 10^{23} \text{ Hz } \alpha^{-1} (1+Y_e)^{-1} (\mathcal{E}_{52}/n)^{1/8} t_h^{-3/8} (1+z)^{-5/8}, \quad (9)$$

$$\nu_{u,p} = 2.8 \times 10^{23} \text{ Hz } \alpha^{-2} \epsilon_B^{3/2} (\mathcal{E}_{52} n)^{3/4} t_h^{-1/4} (1+z)^{-3/4}. \quad (10)$$

Finally, the maximum electron synchrotron flux is $F_{\nu, \text{max}, e} = [(4\pi/3)r^3\zeta_e n \Gamma P'_{\nu'_{m,e}}/4\pi D^2](1+z) = (\phi_0\sqrt{3}/3)(e^3\zeta_e n/mc^2 D^2)\Gamma B'r^3(1+z) = 29 \text{mJy} \zeta_e \epsilon_B^{1/2} n^{1/2} \mathcal{E}_{52} D_{28}^{-2}(1+z)$, where $D \equiv D(z) = 10^{28} \text{cm} D_{28}$ is the proper distance of the source (which, depending on the cosmological model, is also redshift dependent). Similarly, the maximum proton synchrotron flux is $F_{\nu, \text{max}, p} = 15.7 \mu \text{Jy} \zeta_p \epsilon_B^{1/2} n^{1/2} \mathcal{E}_{52} D_{28}^{-2}(1+z)$.

For $\nu < \nu_{u,e}$, the condition for the proton synchrotron component to overcome the electron component is $F_{\nu, p}(\nu_{u,p}) > F_{\nu, e}(\nu_{u,p})$. Using eq.(5,8,10), this translates into

$$(1+Y_e)^{2/3} \epsilon_B > 594(\epsilon_e/\epsilon_p)^{2(p-1)/3} (\zeta_p/\zeta_e)^{2(p-2)/3} \alpha^{2/3} \mathcal{E}_{52}^{-5/12} n^{-7/12} [t_h/(1+z)]^{-1/12}, \quad (11)$$

which is shown as line 1 in Fig. 1.

Another condition for the competition between the p and e components might be thought to be relevant is $\nu_{u,p} > \nu_{u,e}$, which corresponds to $(1+Y_e)^{2/3} \epsilon_B > 0.88 \alpha^{2/3} \mathcal{E}_{52}^{-5/12} n^{-7/12} [t_h/(1+z)]^{-1/12}$. However, this condition may not be essential, since as shown by Böttcher & Dermer (1998) there can be other proton-induced electromagnetic signals extending above this energy, of level comparable to or lower than the proton synchrotron component. These include the synchrotron radiation from the positrons produced by π^+ decay and the γ -rays produced directly from π^0 decay. These components may be regarded as an extension to the proton synchrotron component, which would stick out above the electron synchrotron component even if $\nu_{u,p} < \nu_{u,e}$. However, these proton components will compete with the electron IC component, which we discuss in §4.

4. Inverse Compton component

The inverse Compton (IC) is mainly important for the electron component, both for the electron cooling and for forming a separate high energy emission component². The condition for the IC cooling to be important is $\eta \epsilon_e / \epsilon_B > 1$, which has been explicitly addressed by Sari & Esin (2001). Here we investigate the condition that the IC emission component overtakes the electron and/or the proton synchrotron component.

The IC component has a similar spectral shape to the synchrotron component, but its low energy peak is Lorentz-boosted by roughly a factor of $\gamma_{m,e}^2$, while the frequency spread where it is important is stretched out, by comparison to the spread of the synchrotron spectrum, extending between the boosted characteristic and cooling frequencies. Sari & Esin (2001) have explicitly presented analytic expressions for the IC spectral component, and found that the power law approximation is no longer accurate at $\nu > \gamma_m^2 \nu_{m,e}$, since electrons with a range of Lorentz factors between γ_m and γ_c contribute equally to the emission at each frequency. For the convenience of the following discussions, we will still adopt the broken power law approximation

²The IC of the protons is not important since $\eta_p = (\gamma_{m,p}/\gamma_{c,p})^{p-2} \ll 1$.

to perform order-of-magnitude estimations, bearing in mind that more accurate expressions would be necessary in more detailed calculations.

In this approximation, the IC spectral component can be represented (Sari & Esin, 2001) by a four-segment broken power law with power indices ordered from low to high frequency of [1, 1/3, -(p-1)/2, -p/2] in the slow-cooling regime, or of [1, 1/3, -1/2, -p/2] in the fast-cooling regime. The break frequencies are $\nu_{a,e}^{\text{IC}} = \gamma_{m,e}^2 \nu_{a,e}$, $\nu_{m,e}^{\text{IC}} \simeq \gamma_{m,e}^2 \nu_{m,e}$, and the IC cooling frequency $\nu_{c,e}^{\text{IC}} \simeq \gamma_{c,e}^2 \nu_{c,e}$. The maximum flux of the inverse Compton component is roughly a factor $(u'_{ph}/u'_B)(\nu_{m,e}/\nu_{m,e}^{\text{IC}})$ of that of the synchrotron component, where $u'_{ph} \simeq (4/3)c\sigma_{T,e}u'_B\gamma_e^2 \cdot (r/\Gamma c) \cdot (4\Gamma\zeta_e n)$ and $u'_B = B'^2/8\pi$ are the comoving synchrotron photon and magnetic field energy densities, respectively. This gives

$$\frac{F_{\nu,max,e}^{\text{IC}}}{F_{\nu,max,e}} \sim \frac{16}{3}\sigma_{T,e}\zeta_e nr = 3.5 \times 10^{-7}\zeta_e nr_{17} = 5.7 \times 10^{-7}\zeta_e \mathcal{E}_{52}^{1/4} n^{3/4} [t_h/(1+z)]^{1/4}. \quad (12)$$

This shows that generally the IC component can only overtake the synchrotron component beyond the synchrotron component's cooling break, but before the IC component's cooling break. In the slow-cooling regime, for a frequency ν satisfying $\nu_{c,e} \leq \nu \leq \nu_{u,e}$ and $\nu_{m,e}^{\text{IC}} \leq \nu \leq \nu_{c,e}^{\text{IC}}$, the flux ratio of the IC and the synchrotron components is

$$\frac{F_{\nu,e}^{\text{IC}}(\nu)}{F_{\nu,e}(\nu)} = \left(\frac{F_{\nu,max,e}^{\text{IC}}}{F_{\nu,max,e}} \right) \left(\frac{\nu_{m,e}^{\text{IC}}}{\nu_{m,e}} \right)^{(p-1)/2} \left(\frac{\nu}{\nu_{c,e}} \right)^{1/2}. \quad (13)$$

Alternatively, in the fast-cooling regime, for a frequency ν satisfying $\nu_{m,e} \leq \nu \leq \nu_{u,e}$ and $\nu_{c,e}^{\text{IC}} \leq \nu \leq \nu_{m,e}^{\text{IC}}$, the flux ratio of the IC and the synchrotron components is

$$\frac{F_{\nu,e}^{\text{IC}}(\nu)}{F_{\nu,e}(\nu)} = \left(\frac{F_{\nu,max,e}^{\text{IC}}}{F_{\nu,max,e}} \right) \left(\frac{\nu_{c,e}^{\text{IC}}}{\nu_{c,e}} \right)^{1/2} \left(\frac{\nu}{\nu_{m,e}} \right)^{(p-1)/2}. \quad (14)$$

Similarly to the proton synchrotron case, the conditions that the IC component overcomes the synchrotron component is $F_{\nu,e}^{\text{IC}}(\nu_{c,e}^{\text{IC}}) > F_{\nu,e}(\nu_{c,e}^{\text{IC}})$ for the slow-cooling case, or $F_{\nu,e}^{\text{IC}}(\nu_{m,e}^{\text{IC}}) > F_{\nu,e}(\nu_{m,e}^{\text{IC}})$ for the fast-cooling case, and both conditions can be simplified to

$$\frac{16}{3}\sigma_{T,e}\zeta_e nr \gamma_{c,e} \gamma_{m,e}^{(p-1)} > 1. \quad (15)$$

Using eqs.(6) and (7), this IC-dominance condition over electron synchrotron can be re-expressed as

$$(1+Y_e)\epsilon_B < 3.8(\epsilon_e/\zeta_e)^{(p-1)}\zeta_e(\mathcal{E}_{52}/n)^{(p-2)/8} [t_h/(1+z)]^{-3(p-2)/8}. \quad (16)$$

This is the line labeled 2 in Fig. 1. We see that a large ϵ_e or a small ϵ_B makes the IC component more prominent, since a large ϵ_e enhances $\gamma_{m,e}$ and a small ϵ_B tends to increase $\gamma_{c,e}$ due to the inefficient synchrotron cooling. A denser medium also favors the IC component (eq.[12]). One comment is that if one takes into account the flux increase above $\nu_{m,e}^{\text{IC}}$ due to the logarithmic term from the scattering contributions of the different electrons (Sari & Esin 2001), the IC dominance condition is less stringent than (16).

The cut-off energy in the IC component is defined by $\nu_{u,e}^{\text{IC}} = \text{Min}(\gamma_{u,e}^2 \nu_{u,e}, \nu_{\text{KN},e}^{\text{IC}})$, where $\nu_{\text{KN},e}^{\text{IC}}$ is the Klein-Nishina limit. A rough estimate of this frequency is given by $\nu_{\text{KN},e}^{\text{IC}} \sim \gamma_{\text{KN},e}^2 \nu_{\text{KN},e}$, where $\nu_{\text{KN},e} \simeq (\frac{4}{3}\Gamma) \frac{3}{4\pi} \frac{eB'}{m_e c} \gamma_{\text{KN},e}^2$, and $\gamma_{\text{KN},e} \sim mc^2 / \text{Min}(h\nu'_{m,e}, h\nu'_{c,e})$. In any case, the condition $\nu_{u,e}^{\text{IC}} \gg \nu_{u,e}$ always holds, which means that above $\nu_{u,e}$ the IC component always sticks out.

In the ϵ_e, ϵ_B space (Fig.1), we see that the regions defined by (11) and (16) do not overlap. This means that for frequencies $\nu < \nu_{u,e}$, given a certain set of parameters, only one or the other high energy component (IC or proton synchrotron) competes with the electron synchrotron component. We note that there is also a substantial region of parameter space in which neither of these high energy components can be dominant. For frequencies $\nu > \nu_{u,e}$, on the other hand, there is an overlap of the proton dominated phase space region with the IC dominated phase space region in the ϵ_e, ϵ_B plane. We thus need to compare the relative importance of these two components. Below, we choose the slow-cooling case as an example. The fast-cooling case can be discussed in a similar way and results in qualitatively similar conclusions.

Within the slow-cooling regime, there are two cases. If $\nu_{u,e} < \nu < \nu_{c,e}^{\text{IC}}$, the IC emission is important, and one can use eqs. (5), (12) and (13) to define the condition that the proton component overcomes the IC component, i.e., $F_{\nu,p}(\nu)/F_{\nu,e}^{\text{IC}}(\nu) = (\epsilon_p/\epsilon_e)^{(p-1)} (\zeta_e/\zeta_p)^{(p-2)} (m_e/m_p)^{(3p-1)/2} / [(16/3)\sigma_{T,e}\zeta_e nr\gamma_{m,e}^{(p-1)}] > 1$ ³. This can be translated into

$$\epsilon_e < 8.1 \times 10^{-4} \epsilon_p^{\frac{1}{2}} \zeta_e^{\frac{p-2}{p-1}} \zeta_p^{-\frac{p-2}{2(p-1)}} \mathcal{E}_{52}^{-\frac{p+1}{16(p-1)}} n^{-\frac{7-p}{16(p-1)}} [t_h/(1+z)]^{\frac{3p-5}{16(p-1)}}. \quad (17)$$

This is line 3 in Fig. 1, to the left of which proton synchrotron dominates over IC, which again is a relatively small phase space region in terms of ϵ_e (but larger than the region left of line 1, where proton synchrotron dominates over electron synchrotron).

The second case in the slow-cooling regime is for $\nu > \nu_{c,e}^{\text{IC}}$, and here the competition between the two components is more difficult to quantify. The fact that usually $\nu_{u,p} \ll \nu_{u,e}^{\text{IC}}$ would seem to indicate that the proton component is not important. However, as Böttcher & Dermer (1998) have shown, photo-meson interactions between the relativistic protons and the low energy photon spectrum lead to additional hadron-related spectral components at high energies, with a νF_ν level which can be a substantial fraction of that of the proton synchrotron component, but extending to much higher energies. For our purposes it is not necessary here to compute these components in detail, assuming instead as a rough estimate that beyond the maximum proton synchrotron frequency $\nu_{u,p}$ the extended hadron component νF_ν flux level represents a fraction $k = 0.1k_{-1}$ of the proton synchrotron flux level at the proton synchrotron cut-off, $F_{\nu,p}(\nu_{u,p}) = F_{\nu,\text{max},p}(\nu_{u,p}/\nu_{m,p})^{-(p-1)/2}$, so that one has $F_{\nu,p}(\nu)/F_{\nu,p}(\nu_{u,p}) = 0.1k_{-1}(\nu_{u,p}/\nu)$. This is consistent with Böttcher & Dermer's Fig.1, and

³Here we have assumed a $-(p-1)/2$ slope for the proton component extending to infinity. When $\nu > \nu_{u,p}$, this is an over-estimate for the other hadron-related components (Böttcher & Dermer 1998). Thus the real criterion is even more stringent than (17).

in general $k = 0.1k_{-1}$ represents an overestimate of the flux level from these hadron-related components. We then compare $F_{\nu,p}(\nu)$ to $F_{\nu,e}^{\text{IC}}(\nu) = F_{\nu,\text{max},e}^{\text{IC}}(\nu_{c,e}^{\text{IC}}/\nu_{m,e}^{\text{IC}})^{-(p-1)/2}(\nu/\nu_{c,e}^{\text{IC}})^{-p/2}$. Again with the help of (5), (12) and (13), and noticing $F_{\nu,e}^{\text{IC}}(\nu)/F_{\nu,e}^{\text{IC}}(\nu_{c,e}^{\text{IC}}) = (\nu/\nu_{c,e}^{\text{IC}})^{-p/2}$ and $F_{\nu,e}(\nu_{u,p})/F_{\nu,e}(\nu_{c,e}^{\text{IC}}) = (\nu_{u,p}/\nu_{c,e}^{\text{IC}})^{-p/2}$, one can get $F_{\nu,p}(\nu)/F_{\nu,e}^{\text{IC}}(\nu) = [F_{\nu,p}(\nu)/F_{\nu,p}(\nu_{u,p})] \cdot [F_{\nu,p}(\nu_{u,p})/F_{\nu,e}(\nu_{u,p})] \cdot [F_{\nu,e}(\nu_{u,p})/F_{\nu,e}(\nu_{c,e}^{\text{IC}})] \cdot [F_{\nu,e}(\nu_{c,e}^{\text{IC}})/F_{\nu,e}^{\text{IC}}(\nu_{c,e}^{\text{IC}})] \cdot [F_{\nu,e}^{\text{IC}}(\nu_{c,e}^{\text{IC}})/F_{\nu,e}^{\text{IC}}(\nu)] = (\epsilon_p/\epsilon_e)^{(p-1)}(\zeta_e/\zeta_p)^{(p-2)}(m_e/m_p)^{(3p-1)/2}/[(16/3)\sigma_{T,e}\zeta_e nr\gamma_{m,e}^{(p-1)}] \cdot (\nu_{u,p}/\nu_{c,e}^{\text{IC}})^{1/2}(\nu/\nu_{u,p})^{(p-2)/2}$. After some further derivations, the condition $F_{\nu,p}(\nu) > F_{\nu,e}^{\text{IC}}(\nu)$ can be translated into

$$(1 + Y_e)^{0.85}\epsilon_B > 215k_{-1}^{-0.43}\epsilon_e^{1.02}\epsilon_p^{-0.51}\zeta_e^{-0.17}\zeta_p^{0.09}\alpha^{0.34}\mathcal{E}_{52}^{-0.22}n^{-0.35}t_h^{-0.10}(1 + z)^{0.01}\nu_{26}^{-0.04}. \quad (18)$$

These are the lines labeled 4 (calculated for $k = 0.1$) and 4' (for $k = 1$) in Fig. 1. In the above expression we have adopted $p = 2.2$ for both electrons and protons in order to avoid an unnecessarily complicated expression. (The explicit spectral index p -dependence can be written out straightforwardly, and is presented in the Appendix). Notice that this criterion is mildly dependent on ν , and we have adopted $\nu = 10^{26}\text{Hz}$ ν_{26} for the typical frequency in (18). Above this frequency (several TeV), the self-absorption due to $\gamma - \gamma$ pair production becomes important (§5) and the comparison is no longer meaningful. For lower frequencies, the constraint on the hadron-dominant region of parameter space is more stringent.

In summary, the competition between various components in the ϵ_e, ϵ_B diagram can be read off from Fig. 1. A) The first case, applicable to frequencies $\nu < \nu_{u,e}$, is shown by the solid lines (eqs.[11] and [16]), which divide the space into three regions, in which the proton synchrotron component competes with the electron synchrotron component, and the electron synchrotron competes with the the electron IC component, respectively. Regions I and II are the regions where the proton component and the electron IC component dominate in the spectrum, respectively, while in region III, neither of these high energy spectral components can overcome the electron synchrotron component. B) The second case, applicable to frequencies $\nu > \nu_{u,e}$, is shown by the dashed lines dividing the parameter space into two regions, in which the proton synchrotron and the electron IC components compete with each other. Region I' is where the proton component as well as other hadron-related components may overcome the electron IC emission component, while region II' is the IC-dominated region. The dashed line 3 (eq.[17]) is the separation line for the case of $\nu < \nu_{c,e}^{\text{IC}}$, and the dashed line 4 (eq.[18]) is the separation line for the case of $\nu > \nu_{c,e}^{\text{IC}}$, calculated for a typical frequency $\nu \sim 10^{26}$ Hz. For lower frequencies, this line moves leftwards, causing the hadron-dominant phase space region to shrink. It can be seen that the hadron-related components are usually masked by the electron IC component, unless ϵ_e is very small. We note that both eqs.(17) and (18) are derived under conditions which are maximally favorable for the proton components, which includes also adopting the extreme case of $\epsilon_p = 1$, which may be an over estimate (Vietri 1997). Bearing all these facts in mind, we expect that the actual proton-dominated regimes (I and I') could be even smaller than what is indicated in Fig.1. On the other hand, in both the low energy band ($\nu < \nu_{u,e}$) and in the high energy band ($\nu > \nu_{u,e}$), the IC component is important in a much larger portion of the parameter phase space (regions II and II').

5. $\gamma\gamma$ pair attenuation

For the higher energy observer frame GRB photons, the comoving frame photon energy exceeds mc^2 , and for sufficient high photon densities, a photon with energy E in the observer frame may be attenuated by pair production through interaction with softer photons whose energy (also in the observer frame) is equal to or greater than $E_{an} = (\Gamma mc^2)^2/E(1+z)^2$, depending on the impact angle between the two photons. This may greatly degrade the high-energy fluence level, and the corrections due to this $\gamma - \gamma$ absorption process needs to be taken into account. The $\gamma - \gamma$ absorption in the GRB prompt phase has been studied by several authors, e.g. Krolik & Pier 1991; Fenimore et al. 1993; Woods & Loeb 1995; Baring & Harding 1997; Lithwick & Sari 2001. Here, however, instead of the prompt phase we concentrate on the afterglow phase.

To treat the absorption in the afterglow phase we adopt the analytical approach developed for internal shocks by Lithwick & Sari (2001, their eq.[2]), which we adapt here to the external shock scenario. Instead of using δT (the temporal variation timescale in the internal shock scenario), we use in our case an emission timescale $t/(1+z)$, which is the expansion time as viewed by the earth observer with the cosmological time dilation effect correction. Assuming that the emission spectrum around $E_{an} = h\nu_{an}$ is $L_\nu(\nu) = L_{\nu,0}(\nu/\nu_{an})^{-\beta}$, the total photon number with $E > E_{an}$ can be estimated as $N_{>E_{an}} \sim \int_{\nu_{an}}^{\infty} (L_{\nu,0}/h\nu)(\nu/\nu_{an})^{-\beta} d\nu \cdot t/(1+z) = L_\nu(\nu_{an})[t/(1+z)]/h\beta$. Noticing that the average $\gamma\gamma$ cross section is approximately $\frac{11}{180}\sigma_{T,e}$ (Lithwick & Sari 2001), and that $L_\nu(\nu_{an}) = F_\nu(\nu_{an}) \cdot 4\pi D^2/(1+z)$, the attenuation optical depth can be expressed as

$$\tau_{\gamma\gamma}(\nu) = \frac{\frac{11}{180}\sigma_{T,e}N_{>E_{an}}}{4\pi[4\Gamma^2 ct/(1+z)]^2} = \frac{\frac{11}{180}\sigma_{T,e}F_\nu(\nu_{an})D^2}{16\Gamma^4 c^2 h\beta t}, \quad (19)$$

where in terms of the quantities t and $F_\nu(\nu_{an})$ as measured by an Earth observer, the redshift factor has cancelled out.

It is seen from eq. (19) that the dominant spectral dependence of $\tau_{\gamma\gamma}(\nu)$ is on $F_\nu(\nu_{an})$. For $E \sim 1$ TeV (where absorption becomes important), we find $E_{an} \sim 2.6\text{keV } \Gamma_2^2(1+z)^{-2}$, which is above $h\nu_{c,e}$. In this band, the electron synchrotron emission component dominates in a large region of phase space (Fig.1), and even if the IC component may potentially dominate, this happens at a later time (§6), when the GeV-TeV emission is not important. Thus for the regime we are interested in, we can approximate $F_\nu(\nu_{an}) = F_{\nu,max,e}(\nu_{c,e}/\nu_{m,e})^{-(p-1)/2}(\nu_{an}/\nu_{c,e})^{-p/2}$, and take $\beta = p/2$. For the model of the dynamics adopted in this paper and using $p = 2.2$, eq.(19) reads then

$$\tau_{\gamma\gamma}(\nu) \sim 0.34(1+Y_e)^{-1}(1+z)^{(7p-8)/8}\epsilon_B^{(p-2)/4}\epsilon_e^{p-1}\zeta_e^{-(p-2)}\mathcal{E}_{52}^{(p+4)/8}n^{(p+4)/8}t_h^{(8-3p)/8}\nu_{26}^{p/2}, \quad (20)$$

where the dependence of $(1+Y_e)^{-1}$ may be dropped for the regime I bursts ($\epsilon_e \ll \epsilon_B$ and $Y_e \sim 0$). Notice the mild dependence on ν and the weak dependence on t . The absorption becomes important only when ν approaches 1 TeV ($\sim 2.4 \times 10^{26}$ Hz). This simple treatment is in qualitative agreement with the more detailed simulations of Dermer et al. 2000b (their Fig.3).

An approximate expression for the final spectral flux including $\gamma\gamma$ attenuation is given by the flux escaping from a skin-depth of unit optical depth, or

$$F_\nu^{ab}(\nu) = F_\nu^{tot}(\nu)/(1 + \tau_{\gamma\gamma}), \quad (21)$$

where $F_\nu(\nu)^{tot}$ includes the contributions from all the spectral components discussed above.

6. Results and implications for high energy observations

With a simple numerical code that includes the three spectral components discussed in this paper, as well as the $\gamma\gamma$ attenuation effect modeled through eq.(19), we have investigated the spectra and the lightcurves in various energy bands for different choices of the most relevant parameters, especially ϵ_e and ϵ_B . Because of the relatively small value of $\tau_{\gamma\gamma}$ for most energies of interest here, we have treated this as a simple absorption process and have neglected for simplicity the effects of the secondary pairs which it produces. The results generally confirm the division of the ϵ_e, ϵ_B phase space sketched in Fig.1. Below we present some examples and explore the detectability of the proton component and the IC component in the afterglow phase in various bands, in particular at GeV energies with future missions such as *GLAST*, and in the X-ray band with the *Chandra* X-ray Observatory. The signatures of the IC and proton components may be detected at high energies in at least two ways. One is through snapshot spectral fits, which require a wide and well-sampled energy coverage, including the MeV to GeV band. Such simultaneous measurements may be achieved in the *Swift* and *GLAST* era. Another, simpler way, is to study the lightcurves at some fixed high energy band, looking for a possible hardening of the lightcurve, the details of which we discuss below.

6.1. Detectability of the proton synchrotron component

To explore the detectability of the proton synchrotron component, we choose as typical parameters for the regimes I and I' the values $\epsilon_B = 0.5\epsilon_{B,.5}$, $\epsilon_e = 10^{-3}\epsilon_{e,-3}$ and $n = 10^2 n_2$. Notice that $\epsilon_B = 0.5\epsilon_{B,.5}$, $\epsilon_e = 10^{-3}\epsilon_{e,-3}$ would fall outside region I for the density $n \sim 1$ assumed in our Fig. 1, but adopting here a higher density $n_2 \sim 1$ these parameters are appropriate for region I. A denser medium will reduce $\nu_{c,e}$ (eq.[8]) and consequently enlarges the region I (eq.[11]). We do not explore an even lower ϵ_e , since it is unlikely to have values $\epsilon_e \lesssim m_e/m_p \sim 0.5 \times 10^{-3}$.

For the frequency range $\nu < \nu_{u,e}$, the critical time t_p at which the proton component overtakes the electron component, t_p , can be derived by making eq.(5) greater than unity. From eq.(8), and taking a certain band, e.g., $\nu = 10^{23}$ Hz ν_{23} , one gets

$$t_p = 1.1 \text{ hr } \epsilon_{B,.5}^{-3} (\epsilon_{e,-3}/\epsilon_p)^{4(p-1)} (\zeta_p/\zeta_e)^{4(p-2)} \mathcal{E}_{52}^{-1} n_2^{-2} (1+z)^{-3} \nu_{23}^{-2}. \quad (22)$$

The dependence on n is steep, so that for a lower density medium the overtaking time t_p could be too late for observational purposes. The dependence on the frequency is also very steep, so that

the overtaking time for slightly higher ν shifts to much shorter time. For example, for $\nu_{23} = 10$ (4 GeV), the overtaking time moves down to $t_p \sim 40$ s.

Equation (22) indicates that for the above set of parameters, the proton synchrotron component will show up in the GeV band. The possibility of directly detecting this component is interesting for several reasons. One is in possibly providing a constraint on the ratio of the proton to the electron injection fractions into the acceleration process, ζ_p/ζ_e , which is of interest of the shock physics. This would also have important implications for the overall energetics of the fireball. A detection might also provide information on whether the index p is the same for electrons and protons, as assumed here for simplicity (but departures from which would be interesting). We note, however, that the absolute luminosity of this proton GeV emission is too faint to be detected at the typical cosmological distance, e.g., $z \sim 1$ with *GLAST*, although closer sources, e.g., $z \sim 0.1$, are detectable (see §6.4 and Fig.4). Furthermore, the GeV band is just the fuzzy region where both the electron and the proton synchrotron components can cut off (see eqs. [9], [10]), which could result in more complicated behaviors in the GeV lightcurves.

In the X-ray band where *Chandra* is sensitive ($\nu \sim \nu_{18}$), because of the steep frequency dependence $t_p \propto \nu^{-2}$ the overtaking time occurs always too late, when the flux is low. Thus it appears impossible to detect the proton synchrotron component in the X-ray band. Figure 2a shows the snapshot spectra including the X-ray and GeV region for the typical parameter set representative of regime I, with a relatively dense external medium ($n_2 \sim 1$).

One remark is that the condition for the proton synchrotron component to dominate a certain high energy band is that $\nu_{c,e}$ must decrease with time, to make the electron component relatively less prominent (see eq.[5]). This is not the case for the afterglow evolution in a wind-like external medium with $n \propto r^{-2}$ (Chevalier & Li 1999). Thus, a detection of the proton component in the GeV band lightcurve would provide a diagnostic for an approximately constant external medium. A non-detection, however, would not necessarily be an argument against the constant medium, since the phase space region for the proton component detection is small.

6.2. Detectability of the electron IC component

To explore the detectability of the IC component, we choose the typical parameters for regions II and II' to be $\epsilon_B = 10^{-2}\epsilon_{B,-2}$, $\epsilon_e = 0.5\epsilon_{e,.5}$ and $n = 1$, similarly to Sari & Esin (2001). Following the same procedure to derive (22), one can derive the critical time t_{IC} when the IC component overtakes the synchrotron component at a typical frequency $\nu < \nu_{u,e}$.

In the X-ray band, the overtaking time of the IC component usually occurs in the slow-cooling regime, which we will assume in the following discussions (see below). The crossing point between the synchrotron spectral component and the IC spectral component, ν_e^{IC} (Sari & Esin 2001), could in principle be either above or below $\nu_{m,e}^{IC}$. If $\nu_e^{IC} > \nu_{m,e}^{IC}$, eq.(13) could be used directly, and

the overtaking condition is $(16/3)\sigma_{T,e}\zeta_e nr\gamma_{m,e}^{(p-1)}(\nu/\nu_{c,e})^{1/2} > 1$. The complication in comparing the regions I and I' is that the Compton cooling factor $(1+Y_e)$ in the expression of $\nu_{c,e}$ (eq.[8]) can no longer be neglected. For $(\eta\epsilon_e/\epsilon_B)^{1/2} \gg 1$, one has $(1+Y_e) \simeq (\eta\epsilon_e/\epsilon_B)^{1/2}$, where in the slow cooling phase $\eta = (\gamma_{m,e}/\gamma_{c,e})^{p-2}$. We have derived the overtaking time for this case, where $t_{\text{IC}} \propto \nu^{[4(4-p)/(3p^2-23p+36)]}$ (cf. Sari & Esin 2001). For reasonable values of p (e.g. 2.2-2.4), the quantity $(3p^2 - 23p + 36)$ is close to zero, causing a very sharp, and probably unphysical, dependence of t_{IC} on all parameters. However, the value of t_{IC} derived in this manner is not generally useful for our purposes here. The reason is that, to ensure $\nu_e^{\text{IC}} > \nu_{m,e}^{\text{IC}}$, the ϵ_e and ϵ_B should be close to the values near the boundary between the regions II and III (eq.[16]), so that both values are comparable. In such a regime, the approximation of $(1+Y_e) \simeq (\eta\epsilon_e/\epsilon_B)^{1/2}$ no longer holds, and one cannot get a simple analytic expression for t_{IC} .

More generally, the overtaking occurs when $\nu_e^{\text{IC}} < \nu_{m,e}^{\text{IC}}$ in situations where $\epsilon_e \gg \epsilon_B$, as is the case for the typical values adopted above (and in Sari & Esin 2001). Noticing that in this regime $F_{\nu,e}^{\text{IC}}(\nu) = F_{\nu,\text{max},e}^{\text{IC}}(\nu/\nu_{m,e}^{\text{IC}})^{1/3} = F_{\nu,\text{max},e}^{\text{IC}}(\nu/\nu_{m,e}^{\text{IC}})^{-(p-1)/2}(\nu/\nu_{m,e}^{\text{IC}})^{(3p-1)/6}$, using eq.(13) the overtaking condition can be written as $(16/3)\sigma_{T,e}\zeta_e nr\gamma_{m,e}^{(p-1)}(\nu/\nu_{c,e})^{1/2}(\nu/\nu_{m,e}^{\text{IC}})^{(3p-1)/6} > 1$. This finally leads to

$$t_{\text{IC}} = 3.4 \text{ days } \epsilon_{e,5}^{0.89} \epsilon_{B,-2}^{0.08} \zeta_e^{1.63} \mathcal{E}_{52}^{-0.06} n^{-0.66} (1+z)^{-0.36} \nu_{18}^{-0.68} \quad (23)$$

for $p = 2.2$ and $\nu = 10^{18} \text{ Hz } \nu_{18}$ (X-ray band). The p -dependence in the above expression is more cumbersome, and is given in the Appendix. This result is in general agreement with Sari & Esin (2001)⁴, and in addition here we have explicitly presented the ζ_e , \mathcal{E}_{52} , and ν dependences which are absent in their paper. A roughly factor of two difference on the overtaking time (~ 7.7 days in their case) may be caused by slightly different coefficients adopted in both works for the $\nu_{m,e}$, $\nu_{c,e}$, $F_{\nu,\text{max},e}$, etc. Nonetheless, this confirms Sari & Esin's finding that in a reasonably dense medium, the IC component can be directly detected by *Chandra* a couple of days after the burst trigger. We note that a substantial flattening of the X-ray light curve for GRB 000926 has been detected by *Chandra* (Piro et al. 2001). Since the proton component cannot show up in the X-ray band under any circumstances, as we argued in §6.1, such a flattening may indicate a direct detection of the IC emission of the electrons. (An alternative interpretation is advanced in Piro et al 2001).

Extensive efforts have been made to determine key fireball parameters such as $\mathcal{E}, \epsilon_B, \epsilon_e, n$ using snapshot spectral fits extending from radio to X-rays on well studied GRB afterglows (e.g. Galama et al. 1998; Wijers & Galama 1999; Panaiteescu & Kumar 2001; Yost et al. 2001). A cautionary point which needs to be stressed about these analyses is that the spectrum which is observed need not be, as is generally assumed, solely due to electron synchrotron radiation, especially when using late time (\gtrsim a couple of days) data in the fitting. According to our results in this paper, as long as the ϵ_e, ϵ_B phase space is in the regions I or III, the standard fitting assumption (i.e. electron synchrotron dominance) is safe, since there are no high energy (proton

⁴The numerical indices in the equation (23) are in agreement with Sari & Esin's results for $p = 2.2$, except the index for $(1+z)$, where we have included an additional factor from the frequency redshift correction, i.e., $-0.36=0.32-0.68$.

or IC) spectral components appearing in the X-ray band. However, in the region II of parameter space (which includes values of ϵ_B, ϵ_e often derived from such fits), the analysis may not be self-consistent, since the X-ray data points may be due the IC component. This caution applies to even earlier snapshot spectral fits, if the burst happens to occur in a denser medium (notice the negative dependence of n on the $-(2/3)(5p - 26)/(3p^2 - 8p - 12)$ index).

The negative dependence on ν_{18} of t_{IC} (the explicit index is $-(2/3)(3p+2)(p-4)/(3p^2-8p-12)$, see also Sari & Esin 2001) indicates that for energy bands above X-rays, the overtaking time is much earlier⁵. In fact, in the GeV band, the IC component dominates almost throughout the entire afterglow phase. For the typical parameter set corresponding to the IC dominated region II, Figure 2b shows the time evolution of the snapshot spectra. For completeness, we present also in Figure 2a the snapshot spectra for the typical parameter set in the proton dominated region I, while Figure 2c shows the snapshot spectra for parameters in the electron synchrotron dominated region III. We can see that in this latter region, neither of the two high energy components is prominent below \sim GeV energies (although at \gtrsim GeV there is a lower level IC component). Two explanations ought to be made about our numerical code. First, to avoid adding up an unphysical component in the electron synchrotron self-absorption band, we have arbitrarily defined the self-absorption cut-off in the proton component. The self-absorption segment in the electron IC component is still plotted with a slope 2 rather than 1 (Sari & Esin 2001) for the convenience of code developing, which does not influence the final broad-band spectrum. Second, at the cut-off frequency of each component, we have adopted a sharp cut-off while a more realistic cut-off should be exponential. The same applies for the sharp jumps in the lightcurves presented in Figs.3 and 4.

In Figure 3, we present the X-ray lightcurves for the typical bursts in the three different regimes. While the regime I and III afterglows show a monotonous decay in this band, we show that the regime II afterglows can show interesting bump features, due to the dominance of the IC component at a later time, in qualitative agreement with Panaitescu & Kumar (2000) and Sari & Esin (2001).

6.3. GeV afterglows and GRB 940217

The extended GeV emission 1.5 hours after the trigger of GRB 940217 detected by *EGRET* (Hurley et al. 1994) indicates that a high energy spectral component can extend into the GeV band for a long period of time, at least in some bursts. In principle, this could be either due to the proton synchrotron emission in the regime I, or due to the electron IC emission in the regime II, or even due to the electron synchrotron emission in the regime III. We will show below that the regime II IC-dominated origin is the more plausible explanation.

⁵At higher energy bands, $\nu_{\text{IC}} < \nu_{m,e}^{\text{IC}}$ may be no longer satisfied, and the overtaking time may occur in the fast-cooling regime. Nonetheless, the negative dependence on ν of t_{IC} generally holds.

The peak energy flux expected from various scenarios can be estimated straightforwardly. For the proton synchrotron in regime I, we have

$$\nu F_{\nu,p}(\text{GeV}) = \nu F_{\nu,max,p} (\nu/\nu_{m,p})^{-(p-1)/2} \sim 1.4 \times 10^{-14} \text{ ergs s}^{-1} \text{ cm}^{-2} \\ \times \epsilon_p^{(p-1)} \zeta_p^{(2-p)} \epsilon_{B,5}^{(p+1)/4} n_2^{1/2} \mathcal{E}_{52}^{(p+3)/4} D_{28}^{-2} (1+z)^{(9-p)/4} t_h^{-3(p-1)/4} \nu_{23}^{(3-p)/2} \quad (24)$$

(see also Fig.2). This is more than one order of magnitude below the calculated level of Böttcher & Dermer (1998) as well as the analytical estimate of Totani (1998). The main discrepancy with both of these results is due to their having adopted $\gamma_{m,p} = \Gamma$, rather than the more accurate lower value we adopted in eq.(1), and also due to the fact that we calculate the flux coefficient using $p = 2.2$ while they use $p = 2$, which further enhances the discrepancy between $\gamma_{m,p}$ and Γ , and which gives a milder ν -dependence. To test this, we have substituted $\gamma_{m,p} = \Gamma$ and $p = 2$ in our code, and this reproduces Böttcher & Dermer's results. We conclude that the correction introduced by using here the more realistic $\gamma_{m,p}$ (eq.[1]) is essential, and that the previous rough estimates using $\gamma_{m,p} = \Gamma$ can overestimate the proton synchrotron flux level. Another feature, which can be seen from eq.(24), is the negative temporal decay of the flux level with the index $-3(p-1)/4 \sim -0.9$, which indicates that even if the proton synchrotron emission flux level is detectable in the early afterglow phase, it will drop with time as time goes by. For the regime III, electron-synchrotron-dominated case, the trend is similar, with a steeper temporal index $-(3p-2)/4 \sim -1.15$ (Fig.4).

In the IC-dominated regime II, contrary to the proton component, the IC component itself has a bump peaking at $\nu_{m,e}^{\text{IC}}$ (for slow-cooling) or $\nu_{c,e}^{\text{IC}}$ (for fast-cooling) in the F_{ν} plot. The peak will sweep the band $\nu = 10^{23} \text{ Hz} \nu_{23}$ at $t = t_{max} \sim 0.3 \text{ hr} \epsilon_{e,5}^{16/9} \zeta_e^{-16/9} \epsilon_{B,-2}^{2/9} \mathcal{E}_{52}^{1/3} n^{-1/9} (1+z)^{5/9} \nu_{23}^{-4/9}$ in the slow-cooling regime. The temporal index before the flux reaches its peak is 1 (slow-cooling) or $(8-3p)/3(4-p) \sim 0.26$ (fast cooling), and is $(11-9p)/8 \sim -1.1$ (slow cooling, which is usually the case) after the flux has passed its peak. The peak energy flux can be estimated as $\nu F_{\nu,max,e}^{\text{IC}}(t = t_{max}) \sim 3.0 \times 10^{-10} \text{ ergs s}^{-1} \text{ cm}^{-2}$ for $\epsilon_B \sim 0.01$ (see also Fig.4). This temporal evolution is mild, which allows a substantial GeV emission component lasting hours after the GRB trigger.

The *EGRET* sensitivity above 100 MeV is $\sim 10^{-7} \text{ ph s}^{-1} \text{ cm}^{-2}$ for point-source observations over a period of two weeks in directions away from the Galactic Plane. Correcting for an effective on-source observing fraction on average of 45% (D. J. Thompson, private communication), the fluence threshold may be estimated as $\sim 10^{-7} \cdot 400 \text{ MeV} \cdot T(t/T)^{1/2} \sim 5 \times 10^{-8} t^{1/2} \text{ ergs cm}^{-2}$, where $T = 14 \cdot 86400 \cdot 45\%$, and t is the integration time in seconds. Such a fluence level is not achievable for regime I or III bursts, but is attainable for a regime II burst located at a closer distance (e.g. $z = 0.1$, see Fig.4), or in a higher density environment. Thus the late (\sim hour) GRB 940217 afterglow was most likely dominated by the electron IC emission from a nearby or dense-medium regime II burst. This agrees with Mészáros & Rees (1994), and Dermer et al. (2000b) drew a similar conclusion by detailed simulations using a specific set of parameters, i.e., $\epsilon_e = 0.5$, $\epsilon_B \leq 10^{-4}$, which lie in our regime II. The Gamma-ray Large Area Space Telescope

(*GLAST*) currently under construction will have a sensitivity of $\sim 1.6 \times 10^{-12} \text{ ergs s}^{-1} \text{ cm}^{-2}$ (Gehrels & Michelson 1999), and will be roughly 40 times more sensitive than *EGRET* in the point-mode, which is a $\sim 1.2 \times 10^{-9} t^{1/2} \text{ ergs cm}^{-2}$ threshold fluence. This will make most regime II burst afterglows detectable at a typical cosmological distance and in a moderate density medium, and make the regime I and regime III burst afterglow detectable at a closer distance (Fig.4).

In Figure 4 we show the GeV lightcurves for bursts typical of the three different parameter regimes. For easier comparison with future observations, we have integrated over the 400 MeV - 200 GeV band to get the total energy fluence *GLAST* can collect during a certain time duration t . The sensitivity threshold of *EGRET* and *GLAST* are indicated. One sees that regime II burst afterglows would be generally detectable by *GLAST* within hours after the burst trigger. Bursts in regime I and III are also detectable by *GLAST* in the prompt phase, if the source is at closer distances, but their flux level will drop with time rapidly below the level of detection. A criterion to differentiate between nearby regime I and III bursts is that the lightcurve for the regime I burst is flatter. We conclude that an extended GeV afterglow is a diagnostic of a regime II (IC-dominated) burst.

Recently, an energy flux upper limit $J(E > 760 \text{ GeV}) < 9.4 \times 10^{-12} \text{ ergs cm}^{-2} \text{ s}^{-1}$ in GRB 010222 was obtained in a 4-hour measurement with the stereoscopic *HEGRA* Cherenkov telescope system, 19 hours after the burst trigger (Goetting & Horns 2001). Given the cosmological distance of $z \geq 1.477$ (Jha et al. 2001), this is consistent with our model prediction in this paper (see Fig.2), even for the most favorable regime II case (Fig.2b).

6.4. Prospects from broadband observations in the *Swift-GLAST* era

The *GLAST* mission will be launched in 2005, with a sensitivity range in the 20 MeV-300 GeV, complemented by the Glast Burst Monitor (*BGM*) whose energy range extends from a few keV to 30 GeV. Another broad band GRB mission, *Swift*, will be launched in 2003, and will be sensitive in the optical, X-ray and γ -rays up to $\lesssim 140$ keV. At the same time, ground-based experiments such as *Milagro*, *HESS*, *Veritas*, *MAGIC* and *Cangaroo-III* may provide $\gtrsim 0.5$ TeV, or in some cases $\gtrsim 30$ GeV data or upper limits. In the *Swift-GLAST* era, simultaneous broad-band observations at the very earliest stages of the GRB afterglows will become possible, which will bring invaluable information about GRB shock physics and the central engine. Here we note two interesting issues which can be addressed in the *Swift-GLAST* era:

1. Sari & Esin (2001) pointed out that due to the IC cooling, there are two possible solutions of the unknown fireball and shock parameters for a same set of observables from the low-energy afterglow fits. These solutions are degenerate, and are indistinguishable with the present data. However, we note that the two sets of solutions lie within the regime III and regime II, respectively. This provides a natural way to distinguish between the two scenarios, by using the GeV afterglow data. If an extended GeV afterglow is detected by *GLAST*, then the parameter space should be in

regime II where the IC component dominates in the high energy band. In this case eqs.(4.17) to (4.20) of Sari & Esin (2001) will apply. Otherwise, the parameter space should be in regime III, where no prominent emission component shows up in the GeV band. This is the case that Sari & Esin's eqs.(4.13) to (4.16) may apply.

2. It has been proposed by Waxman (1995) and Vietri (1995) that GRBs are likely sites to produce ultra-high-energy cosmic rays (UHECRs), and that the 10^{20} eV excess UHECRs detected are of the GRB origin. This hypothesis is subject to debate (cf. Stecker 2000; Mannheim 2000; Scully & Stecker 2001). We note that future GeV observations with *GLAST* may be able to solve this debate, at least for the external shock scenario. To accelerate protons to ultra-high energies around 10^{20} eV, ϵ_B must be close to unity (Waxman 1995; Vietri 1995; Rachen & Mészáros 1998). If substantial extended GeV afterglows are common among GRBs, and if the redshift measurements from the low frequency afterglow observations indicate that the GRBs are around $z \sim 1$, this will impose severe constraints on the UHECR acceleration theory by the external shock scenario, since the regime II generally favors a small ϵ_B . (However, our calculations do not apply to a possible UHECR acceleration in internal shocks). On the other hand, if long duration GeV afterglows are not common, and for a few nearby bursts a GeV (prompt) lightcurve hardening is detected, this could be attributable to proton synchrotron emission, in which case both ϵ_p and ϵ_B are close to unity. This would provide support to the theory of UHECR origin in GRBs. Since these components are not masked by the electron synchrotron and the IC components, this would also hint at a small ϵ_e (e.g. due to a weak coupling between electrons and protons, as argued by Totani 1998; 2000).

7. Summary

We have studied GRB afterglow snapshot spectra and lightcurves over a broader band than usual by including the canonical electron synchrotron emission as well as two other high energy spectral components, i.e., the proton synchrotron emission component and the electron synchrotron self-inverse-Compton emission component. We have in particular concentrated upon the X-ray to GeV-TeV ranges, including the effect of attenuation by $\gamma\gamma$ pair formation. This investigation has the advantage, relative to prior ones, of bringing together in a single coherent treatment the effects of these various high energy mechanisms, which hitherto had been mostly treated singly or in twos, within the context of a specific GRB afterglow dynamical model. This is carried out over a wider range of parameter phase space than hitherto, to allow a global view on the relative importance of the various spectral components.

For the frequency range below the electron's synchrotron cut-off, $\nu < \nu_{u,e}$, there is a competition between the electron synchrotron component on the one hand, and the proton synchrotron component or the electron IC component on the other, which can affect the higher energy bands including X-rays or above. This competition divides the ϵ_e, ϵ_B phase space into three regimes (Fig.1). We have explored the range of validity of these regimes, and discussed

the conditions for which these high energy spectral components would show up in various bands, especially in the GeV and the X-ray band. The conclusion is that the IC component is likely to be important in a relatively large region of parameter space, while the conditions for which the proton synchrotron component is important involve a small, but non-negligible, region of parameter space. One interesting consequence is that there is a substantial region (regime III) in which neither of the two high energy components are important. These bursts, as well as the regime I (proton dominated) bursts may be still detectable by *GLAST* in the prompt afterglow phase due to the electron synchrotron emission if the source is located closer to the earth. Above the electron synchrotron cut-off, the competition is between the electron IC component and the hadron-related photo-meson decay components, which we treated as a reduced extension of the proton synchrotron component. Again, the phase space region where the latter effects are important in the afterglow is small. We also find that for the external shock and the afterglow phase the $\gamma - \gamma$ absorption is not important below the TeV range.

A general conclusion is that the most likely origin for an extended high energy afterglow component at GeV energies is from the electron IC component, at least for the values of ϵ_e, ϵ_B that have been most commonly derived so far from snapshot spectral analyses. Not only is the phase space region where the IC component dominates (II and II') much larger than that where the proton component dominates (I and I', see Fig. 1), but also its intensity is much higher than that of the hadron components, and the time scale during which an appreciable flux level is maintained in the GeV band is much longer than for the hadronic components. In the parameter regime favorable for the IC emission, this component is observable at and above the X-ray band. In the X-ray band, it will lead to a flattening of the light curve at late times, as long as the medium density is not too low (see also Sari & Esin 2001). Above the X-ray band, the time after which IC emission becomes dominant appears earlier, and the IC component dominates the GeV-band emission almost from the onset of the afterglow phase. In general, a high external density medium favors the detectability of the IC component. Such an IC component is likely to have been responsible for the GeV photons detected from GRB 940217 with *EGRET*, and similar events should in the future be detectable by *GLAST*.

The proton synchrotron component, as well as the hadron-related photo-meson electromagnetic components in the afterglow radiation are likely to be, in most cases, less important than previous approximate estimates indicated (Vietri 1997; Böttcher & Dermer 1998; Totani 1998; Totani 2000). The ϵ_e, ϵ_B phase space region where this component overcomes the electron synchrotron and the IC components is very small, unless the medium density is high. Even in the most favorable region of the phase space, the proton component is not expected to show up in the X-ray band, but it may overcome the electron synchrotron component in the GeV band shortly after the onset of the afterglow phase, if the medium density is moderately high. However, the flux level drops with time, and may be only detected by *GLAST* in the very early phase of the afterglow if the source distance is close. Nonetheless, the detection of a proton component is of extremely high interest (§6.1) for the GRB and shock physics. Its detection, if successful, would imply, depending

on its strength, fireball and shock parameters which are more extreme than currently commonly assumed. In particular, it would provide a diagnostic for a high ϵ_p, ϵ_B and/or a low ϵ_e .

We point out a simple way to break the current parameter space degeneracy which currently, from low frequency observations alone (X-rays and below), prevent the unambiguous determination of the unknown fireball and shock parameters, through the use of snapshot spectral measurements extending into the GeV range. We also suggest a way to test the hypothesis of a GRB origin for UHECR using combined *Swift* and *GLAST* data. Such observations will also provide diagnostics for the presence of a quasi-homogeneous versus a wind-like inhomogeneous external medium.

Finally, we note that the condition for the spectral IC component to be prominent (eq.[16] and Fig.1) usually covers the parameter regime in which IC cooling is important ($\eta\epsilon_e/\epsilon_B > 1$, Sari & Esin 2001). Thus, the current snapshot spectral fits ought to be made with caution for the X-ray data points when the IC cooling is important, especially for the data at later times, and for cases which may involve a high external medium density.

We are grateful to C. D. Dermer, D. J. Thompson and M. Böttcher for informative correspondence, and to NASA NAG5-9192 and NAG5-9193 for support.

A. Explicit p -dependences of equations (18) and (23)

In this appendix, we explicitly present the p -dependent indices in equations (18) and (23). For equation (18):

$$(1 + Y_e)^{\frac{8}{16-3p}} \epsilon_B > 215 k_{-1}^{-\frac{4}{16-3p}} \epsilon_e^{\frac{8(p-1)}{16-3p}} \epsilon_p^{-\frac{4(p-1)}{16-3p}} \zeta_e^{-\frac{8(p-2)}{16-3p}} \zeta_p^{\frac{4(p-2)}{16-3p}} \alpha^{\frac{4(3-p)}{16-3p}} \times \mathcal{E}_{52}^{-\frac{13-4p}{2(16-3p)}} n^{-\frac{11-2p}{2(16-3p)}} t_h^{-\frac{4p-7}{2(16-3p)}} (1 + z)^{\frac{9-4p}{2(16-3p)}} \nu_{26}^{-\frac{2(p-2)}{16-3p}}. \quad (A1)$$

For equation (23):

$$t_{\text{IC}} = 3.4 \text{ days} \epsilon_{e,5}^{\frac{4(3p^2-8p-7)}{3(3p^2-8p-12)}} \epsilon_{B,-2}^{\frac{3p^2-10p+4}{3(3p^2-8p-12)}} \zeta_e^{\frac{4(3p^2-5p-22)}{3(3p^2-8p-12)}} \times \mathcal{E}_{52}^{\frac{2p^2-4p+1}{2(3p^2-8p-12)}} n^{-\frac{2(5p-26)}{3(3p^2-8p-12)}} (1 + z)^{-\frac{3p^2-16p+4}{3(3p^2-8p-12)}} \nu_{18}^{-\frac{2(3p+2)(p-4)}{3(3p^2-8p-12)}}. \quad (A2)$$

REFERENCES

Baring, M. G., & Harding, A. K. 1997, ApJ, 491, 663

Böttcher, M., & Dermer, C. D. 1998, ApJ, 499, L131

Chevalier, R. A., & Li, Z.-Y. 1999, *ApJ*, 520, L29

Dermer, C. D., Böttcher, M., & Chiang, J. 2000a, *ApJ*, 537, 255

Dermer, C. D., Chiang, J., & Mitman, K. E. 2000b, *ApJ*, 537, 785

Fenimore, E. E., Epstein, R. I., & Ho, C. 1993, *A&AS*, 97, 59

Freedman, D & Waxman, E, 2001, *ApJ*, 547, 922

Galama, T. J., et al. 1998, *ApJ*, 500, L101

Gehrels, N., & Michelson, P. 1999, *AstroParticle Physics*, 11, 277

Goetting, N., Horns, D. on behalf of the HEGRA Collaboration. 2001, *GCN* 1007

Hurley, K., et al. 1994, *Nature*, 372, 652

Jha, S., et al. 2001, *ApJ Lett.*, submitted (astro-ph/0103081)

Krolik, J. H., & Pier, E. A. 1991, *ApJ*, 373, 277

Lithwick, Y., & Sari, R. 2001, *ApJ*, submitted (astro-ph/0011508)

Mannheim, K. 2000, in H.J. Voelk and F. Aharonian (eds.), *Proc. of the Heidelberg International Symposium on High Energy Gamma-Ray Astronomy*, Heidelberg, June 26-30, 2000, AIP Conf. Proc (astro-ph/0010353)

Mészáros, P., & Rees, M. J. 1994, *MNRAS* 269, L41

—. 1997, *ApJ*, 476, 232

Mészáros, P., Rees, M. J., & Papathanassiou, H. 1994, *ApJ*, 432, 181

Panaitescu, A., & Kumar, P. 2000, *ApJ*, 543, 66

—. 2001, *ApJ*, submitted (astro-ph/0010257)

Panaitescu, A., & Mészáros, P. 1998, *ApJ*, 501, 772

Piro, L., et al. 2001, submitted

Rachen, J. P., & Mészáros, P. 1998, *Phys. Rev. D.*, 58, 123005

Sari, R., & Esin, A. A. 2001, *ApJ*, 548, 787

Sari, R., Piran, T., & Narayan, R. 1998, *ApJ*, 497, L17

Scully, S. T., & Stecker, F. W. 2001, *AstroParticle Physics*, submitted (astro-ph/0006112)

Stecker, F. W. 2000, *AstroParticle Phys.*, 14, 207

Totani, T. 1998, *ApJ*, 502, L13

—. 2000, *ApJ*, 536, L23

van Paradijs, J, Kouveliotou, C & Wijers, R. A. M. J., 2000, *ARA&A*, 38, 379

Vietri, M. 1995, *ApJ*, 453, 883

—. 1997, *Phys. Rev. Lett.*, 78, 4328

Waxman, E. 1995, Phys. Rev. Lett., 75, 386

—. 1997, ApJ, 485, L5

Wei, D. M., & Lu, T. 1998, ApJ, 505, 252

—. 2000, A&A, 360, L13

Wijers, R. A. M. J., & Galama, T. J. 1999, ApJ, 523, 177

Woods, E., & Loeb, A. 1995, ApJ, 453, 583

Yost, S., et al. 2001, in preparation

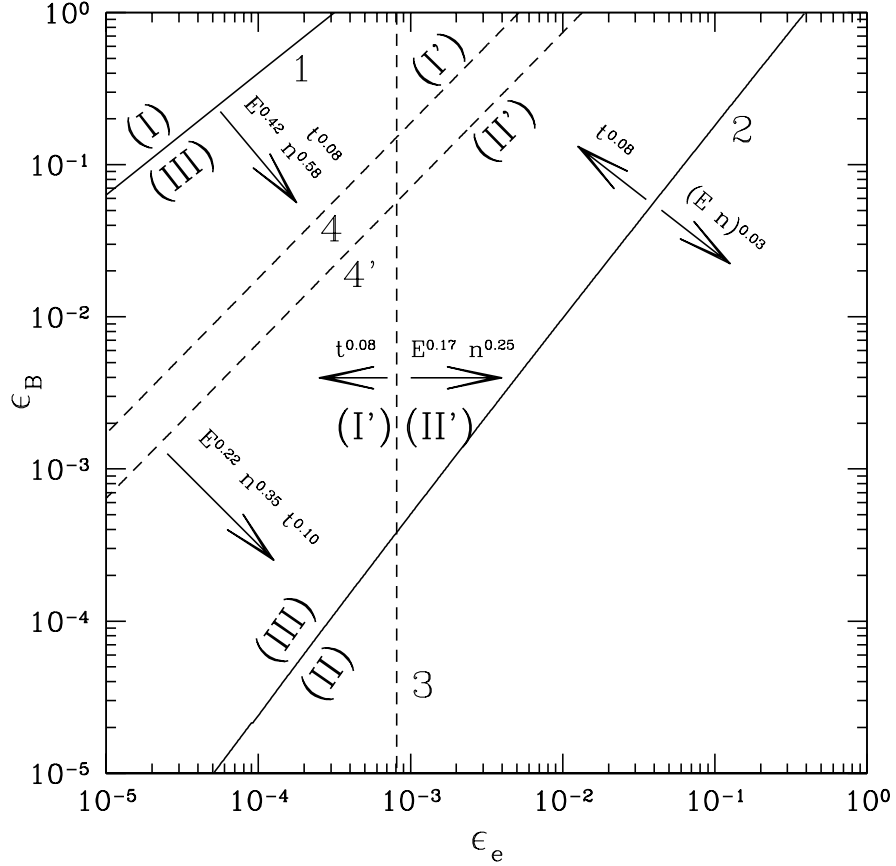


Fig. 1.— Regions in the ϵ_e, ϵ_B parameter space where the various radiation mechanisms dominate at selected frequencies. A) For photon energies $\nu < \nu_{u,e}$ (the synchrotron frequency for electrons at the upper end of their energy distribution) the solid lines 1 and 2 divide the space into three regimes. Regime I is where the proton synchrotron component overcomes the electron synchrotron component; regime II is where the electron IC component overcomes the electron synchrotron component; and regime III is where the electron synchrotron component dominates the other two. B) For a higher energy band with $\nu > \nu_{u,e}$, the space is divided into two regimes I and I' by a dashed line 3, or a dashed line 4 (4'), depending on the subcase. Regime I' is where the proton-related components overcome the electron IC component, and regime II' is where electron IC dominates over the proton components. For $\nu < \nu_{c,e}^{IC}$ (the inverse Compton-boosted frequency of synchrotron photons radiated by electrons at the cooling break energy) the separation is given by line 3, which does not depend on the frequency. For $\nu > \nu_{c,e}^{IC}$ the separation line is frequency-dependent, and given by line 4 (4'), which are drawn for $\nu \sim 10^{26}$ Hz. Line 4 assumes the reduction factor is $k = 0.1$, while line 4' assumes $k = 1$ (see text). The dependences of the separation lines on t , n and \mathcal{E} are indicated on the plot, which cause the different regimes to enlarge or shrink with these parameters. All lines are drawn using the following parameters: $\xi_e = \xi_p = 1$, $\epsilon_p = 1$, $\mathcal{E}_{52} = 1$, $n = 1$, $\alpha = 1$, $z = 1$, $p = 2.2$ and $t = 1$ hr. For a flatter p (close to 2), the lines 1, 2, 4 and 4' are flatter, and the regions I and I' will be slightly enlarged. For a steeper p , the trend is the opposite.

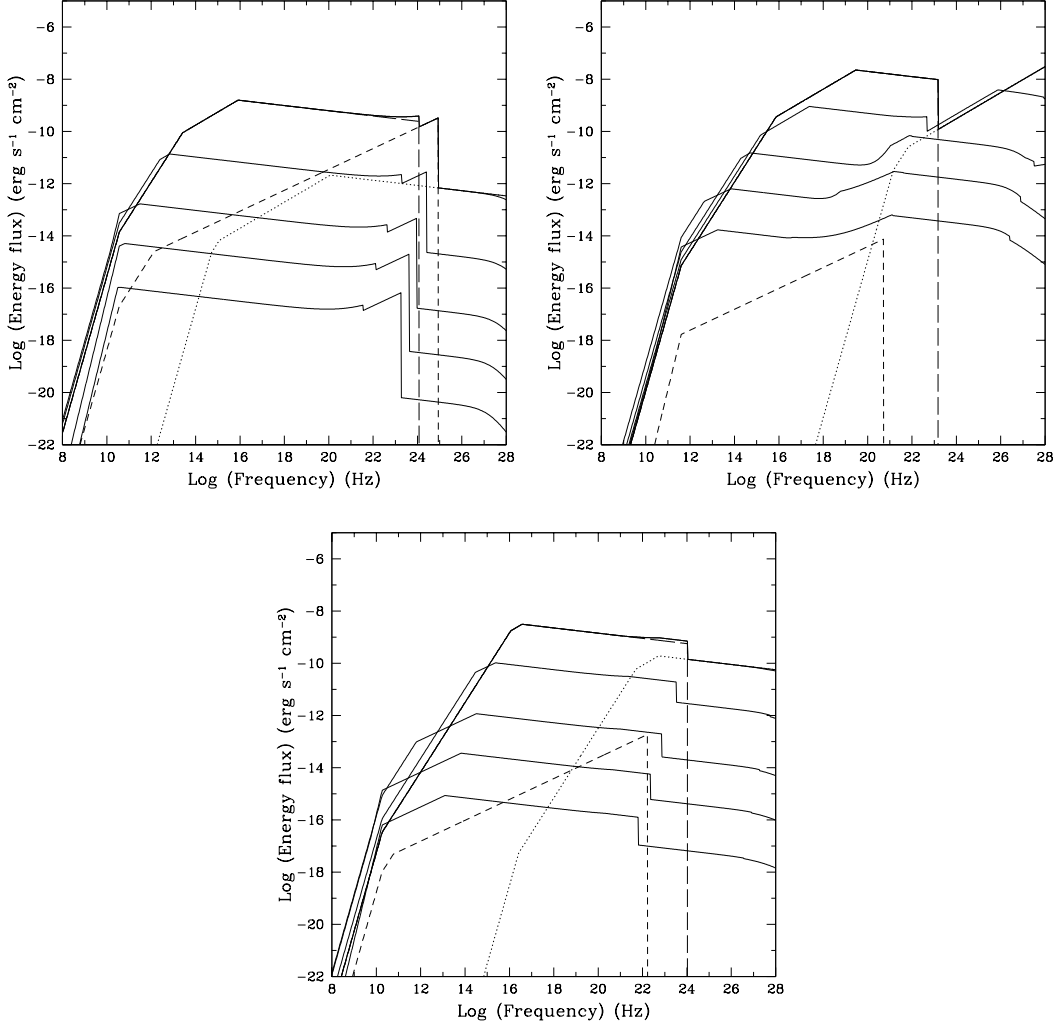


Fig. 2.— Temporal evolution of the broad-band spectra of GRBs. Thick solid curves are the final spectra for various observer times, starting from (top) the onset of the afterglow, 1 minute, 1 hour, 1 day to (bottom) 1 month, respectively. The sharpness of the breaks and cutoffs is an artifact of the analytical approximations, in reality these would be smoother transitions. For the top curve, contributions from the various radiation components are also plotted. Long dashed are electron synchrotron, short dashed are proton synchrotron, and dotted lines are electron inverse Compton emission. The thin solid line is the total energy flux level without $\gamma\gamma$ absorption correction, while the thick solid line is the energy flux level after the $\gamma\gamma$ self-absorption correction. The intergalactic absorption, which also becomes important around $\nu = 10^{26}$, is distance dependent and has not been included in this graph. Here all plots are calculated for standard parameters $z = 1$ (flat, $\Lambda = 0$ universe), $\zeta_e = \zeta_p = 1$, $\epsilon_p = 1$, $\mathcal{E}_{52} = 1$, $\alpha = 1$, $z = 1$, $p = 2.2$, and $\Gamma_0 = 300$, while ϵ_e , ϵ_B and n vary for the different regimes. (a) A typical regime I burst: $\epsilon_e = 10^{-3}$, $\epsilon_B = 0.5$, $n = 100 \text{ cm}^{-3}$. (b) A typical regime II burst: $\epsilon_e = 0.5$, $\epsilon_B = 0.01$, $n = 1 \text{ cm}^{-3}$. (c) A typical regime III burst: $\epsilon_e = 0.01$, $\epsilon_B = 0.1$, $n = 1 \text{ cm}^{-3}$.

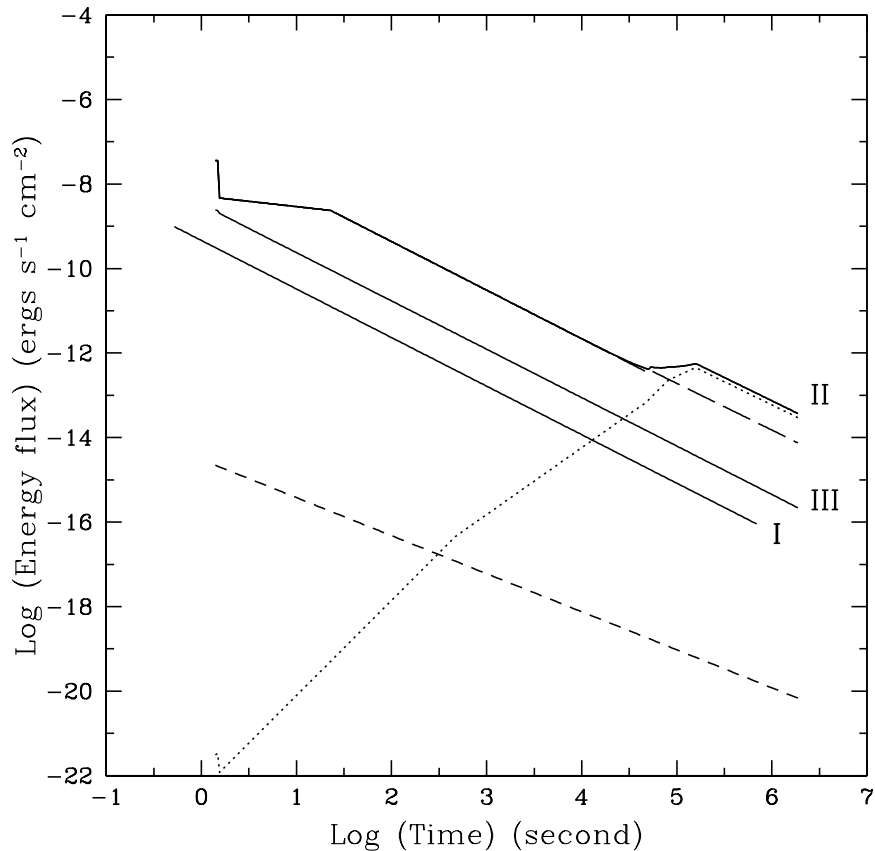


Fig. 3.— X-ray νF_ν lightcurves ($\nu = 10^{18}$ Hz) for the three types of bursts, starting from t_{dec} and ending at the time when the bulk Lorentz factor $\Gamma = 2$. Curves I, II, and III are calculated for regimes where the proton synchrotron, the electron IC, and the electron synchrotron dominate, respectively. All the parameters adopted are the same as those in Fig.2, except for the regime II burst, where a slight denser medium $n = 5\text{cm}^{-3}$ is adopted to show how the IC component flattens the light curve at later times. For the regime II, the contributions from the three different components are also shown with the same notations as in Fig.2.

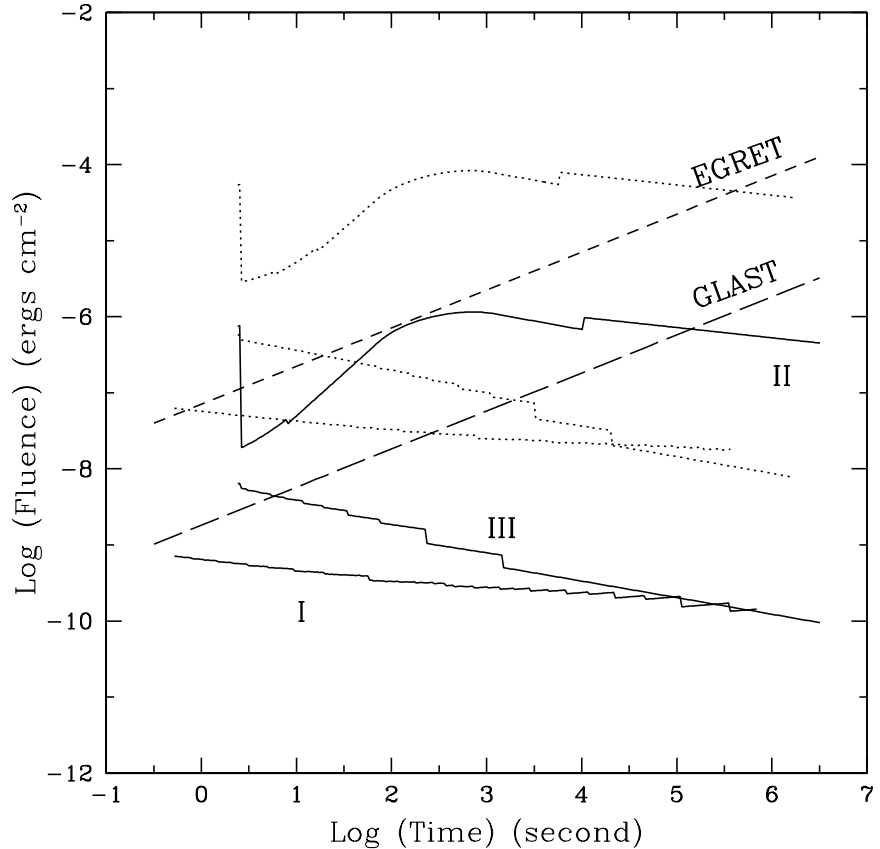


Fig. 4.— GeV $\int_{\nu_1}^{\nu_2} \nu F_{\nu} d\nu \cdot t$ lightcurves for the three types of bursts, starting from t_{dec} and ending at the time when the bulk Lorentz factor $\Gamma = 2$. The energy flux has been integrated within the range of $\nu_1 \sim 400$ MeV to $\nu_2 \sim 200$ GeV in order to compare with observations. The solid curves I, II and III indicate bursts in regimes I, II, and III, respectively, at a typical cosmological distance ($z = 1$, for a flat $\Lambda = 0$ universe). The three dotted unmarked curves are the same types of bursts located at $z = 0.1$. The other parameters adopted are the same as those in Fig.2. The sensitivity curves for *EGRET* and *GLAST* are also plotted. For these parameters, the electron IC component gives an extended duration GeV emission, easily detectable by *GLAST* at $z = 1$ in a regime II burst (solid line). For $z = 0.1$ (dotted lines), *GLAST* would be able to detect all three types of regime bursts.